6. F. Messenguy and E. Dubois, *Mol. Cell. Biol.* **13**, 2586 (1993).
7. J. Bechet, M. Greenson, J. M. Wiame, *Eur. J. Biochem.* **12**, 31 (1970).
8. E. Dubois and F. Messenguy, *Mol. Gen. Genet.* **243**, 315 (1994).
9. C. A. Keleher, C. Goutte, A. D. Johnson, *Cell* **53**, 927 (1988); M. Maher, F. Cong, D. Kindelberger, K. Nasymth, S. Dalton, *Mol. Cell. Biol.* **15**, 3129 (1995).
10. C. Wolberger, *Annu. Rev. Biophys. Biomol. Struct.* **28**, 29 (1999); P. Shore and A. D. Sharrocks, *Eur. J. Biochem.* **229**, 1 (1995).
11. F. Estevez, D. Pulford, M. J. Stark, A. N. Carter, C. P. Downes, *Biochem. J.* **302**, 709 (1994); P. P. Ongusaha, P. J. Hughes, J. Davey, R. H. Mitchell, *Biochem. J.* **335**, 671 (1998).
12. K. Y. Choi *et al.*, *Science* **248**, 64 (1990); D. Communi, V. Vanweyenberg, C. Erneux, *Cell. Signalling* **7**, 643 (1995).
13. The following D-IP isomers were tested: $I(1,4)P_2$, $I(1,3,4)P_3$, $I(1,2,6)P_3$, $I(1,3,4,5)P_4$, $I(3,4,5,6)P_4$, $I(1,3,4,5,6)P_5$, and $IP_6$. For each, <1% of total radioactivity was detected as radiolabeled IP product. During revision of this manuscript, it was reported that GST-Arg82 (referred to as ArgRIII) expressed in human cells possessed $IP_3$ kinase activity [A. Saiardi, H. Erdjument-Bromage, A. M. Snowman, P. Tempst, S. H. Snyder, *Curr. Biol.* **9**, 1323 (1999)].
14. J. Flick and J. Thorner, *Mol. Cell. Biol.* **13**, 5861 (1993); T. Yoko-o *et al.*, *Proc. Natl. Acad. Sci. U.S.A.* **90**, 1804 (1993); W. E. Payne and M. Fitzgerald-Hayes, *Mol. Cell Biol.* **13**, 4351 (1993).
15. Of note, a small peak of $IP_4x$ (similar to that reported in *gsl3-3* strains after shift to 37°C) and a small peak of a novel $IP_5x$ were detected in these strains, indicating that other IP kinases may be present in yeast cells.
16. Genomic sequence encoding *ARG82* was isolated using *Taq* polymerase with yeast genomic DNA as template and oligonucleotide primers containing Bam HI restriction sites. Primers were designed based on yeast genomic DNA sequence (DDBJ/EMBL/GenBank). The resulting fragment was cloned into the Bam HI site of plasmids pRS315 and pRS316. These were transformed into strain SWY1852 (*MATα gle3-3 gle1-2 ade2 ade3 ura3 his3 leu2 trp1* pGLE1/URA3/ADE3/CEN). Rescue of synthetic lethality was tested by monitoring for red and white sectoring of a *gsl3-3 gle1-2* pGLE1/URA3/ADE3/CEN pIPK2/LEU2/CEN strain on yeast extract, peptone, and dextrose (YPD) medium. The same strain was tested for temperature-sensitive growth at 37°C on medium lacking uracil (–Ura). Whereas a pLEU2/CEN plasmid does not confer sectoring on YPD or growth at 37°C on –Ura, the pIPK2/LEU2/CEN plasmid resulted in sectoring and growth at 37°C. Soluble IP levels were analyzed as described above for the *ipk2*Δ strains. Because the haploid *ipk2*Δ strains are defective for mating (*8*), the *ipk2*Δ strain was transformed with pIPK2/URA3/CEN. The resulting haploid was mated with SWY1852 (plus pRS315), and the diploid was assayed for temperature sensitivity after growth on 5-fluoroorotic acid.
17. E. Dubois and F. Messenguy, *Mol. Cell. Biol.* **11**, 2162 (1991).
18. M. d. Rijcke, S. Seneca, B. Punyammalee, N. Glansdorff, M. Crabeel, *Mol. Cell. Biol.* **12**, 68 (1992).
19. A mutant *ipk2* lacking $IP_3$-$IP_4$ kinase activity (*ipk2kin*$^-$) was constructed using a PCR-based mutagenesis strategy that resulted in a single amino acid substitution (replacement of aspartate 131 with alanine). The coding sequence of *ipk2kin*$^-$ was fused in frame to GST, expressed in bacteria, and purified. GST-ipk2kin$^-$ (100 ng) did not exhibit detectable kinase activity toward $IP_3$ and $IP_4$. The coding sequence of *ipk2kin*$^-$ was cloned into pUNI-10 and recombined with GFP-acceptor plasmid (*26*) to generate pGFP-ipk2kin$^-$. Cells lacking *ipk2*Δ were transformed with pGFP-ipk2kin$^-$ (*ipk2*Δ + pIpk2kin$^-$) and analyzed. Expression of GFP-tagged ipk2kin$^-$ restored ArgR-Mcm1 complex formation in *ipk2*Δ strains similar to GFP-tagged Ipk2; however, in contrast to GFP-Ipk2, expression of the GFP-ipk2kin$^-$ mutant was unable to rescue the slow growth at 30°C, inviability at 37°C, inviability on ornithine medium, and $IP_4$ or $IP_5$ production (as measured by steady-state inositol labeling) observed in *ipk2*Δ strains.
20. E. Dubois, J. Bercy, F. Messenguy, *Mol. Gen. Genet.* **207**, 142 (1987).
21. Single-cell plating efficiencies of the relevant strains were determined to confirm the results obtained by streaking cells on ornithine solid medium. Sonicated cultures of known cell number were plated in parallel at multiple dilutions to rich medium versus medium containing ornithine as a sole nitrogen source. Plates were grown at 30°C for 3 to 4 days, and colony-forming units (CFU) were determined by visualization. Percent plating efficiency was defined as (CFU on ornithine medium/CFU on rich medium) × 100. Percent plating efficiency of wild-type cells on ornithine medium was 100%; for *ipk2*Δ, 0%; for *ipk1*Δ, 87%; for *plc1*Δ, <2%; and for *ipk2-3*, 85%. Results are averages obtained from two independent trials. These strains were also plated onto solid medium containing glutamate as the sole nitrogen source, and all strains were able to grow as single colonies having plating efficiencies of greater than 85%. Cells lacking *plc1* or *ipk2* did not exhibit measurable changes in $PI(4,5)P_2$ levels as compared with wild-type using a steady-state radiolabeling analysis. Additionally, *inp51*Δ strains, which exhibit greater than twofold increases in cellular $PI(4,5)P_2$ (*27*), grew normally on ornithine medium.
22. N. Liu, K. Fukami, H. Yu, T. Takenawa, *J. Biol. Chem.* **271**, 355 (1996); M. Yamaga, M. Fujii, H. Kamata, H. Hirata, H. Yagisawa, *J. Biol. Chem.* **274**, 28537 (1999).
23. J. Bercy, E. Dubois, F. Messenguy, *Gene* **55**, 277 (1987).
24. The amino-terminal end of *IPK2* was fused in frame to GFP and expressed from a centromeric *TRP1* plasmid under control of the *CDC42* promoter in an *ipk2*Δ strain (*26*). Cells were grown to logarithmic growth phase in complete minimal medium minus tryptophan in the presence of 1 μg/ml DAPI. Cells were transferred to slides and viewed directly in growth medium using a Zeiss Axioskop microscope (Zeiss, Thornwood, NY) equipped with epiflorescent and differential interference contrast (DIC) optics. The tagged protein was functionally similarly to native Ipk2. Expression of GFP-tagged Ipk2 on a centromeric plasmid (with the *CDC42* promoter) rescues the temperature sensitivity at 37°C, growth on ornithine, and defects in inositol phosphate production (as determined by steady-state labeling and HPLC analysis) of the *ipk2*Δ strain.
25. Supplementary material is available to *Science* Online subscribers at www.sciencemag.org/feature/data/1045815.shl.
26. The *ipk2*Δ + pIPK2 strains were constructed using modifications to the univector system [Q. Liu, M. Z. Li, D. Leibham, D. Cortez, S. J. Elledge, *Curr. Biol.* **8**, 1300 (1998)]. The *IPK2* gene was amplified from wild-type genomic DNA by using the polymerase chain reaction and cloned in frame with a Lox recombination site in pUNI-10. In vitro site-specific recombination with recombinant GST-Cre enzyme joined this resulting vector and yeast host vector pLOX/GFP/TRP1/CEN to create a centromeric *TRP1* plasmid with an amino-terminal GFP-tagged *IPK2*, under transcriptional control of the *CDC42* promoter. pUNI-10 and pLOX/GFP/TRP1/CEN were kindly provided by D. Lew and J. Moskow, Duke University.
27. L. E. Stolz, W. J. Kuo, J. Longchamps, M. K. Sekhon, J. D. York, *J. Biol. Chem.* **273**, 11852 (1998).
28. Crude extracts were obtained by mechanical lysis of yeast cells with glass beads, in the presence of 200 mM Tris (pH 8.0), 10 mM $MgCl_2$, 1 mM EDTA (pH 8.0), 10% glycerol, 10 mM dithiothreitol, and multiple protease inhibitors (500 μM phenylmethylslfonyl fluoride, 5 μg/ml pepstatin A, 1 μg/ml chymostatin, 100 mM *p*-aminobenzamidine, 100 mM ε-aminocaproic acid, 5 μg/ml aprotinin). The relevant promoter region of the *ARG5,6* gene (bases –142 to +15) was amplified by the polymerase chain reaction, gel-purified, and end-labeled with [$\gamma$-$^{32}$P]ATP by the polynucleotide kinase reaction according to manufacturer's instructions. Soluble protein (50 μg) from each strain was incubated with 10,000 cpm of $^{32}$P-labeled probe for 15 min in 4 mM tris (pH 8.0), 30 mM NaCl, 4 mM $MgCl_2$, 5 μM L-arginine, 0.5 μg/ml herring sperm DNA, and 5% glycerol; complexes were resolved by electrophoresis on 5% nondenaturing polyacrylamide gels and visualized by autoradiography.


29. Supported by the Duke University Medical Scientist Training Program (A.R.O.), grants from the American Cancer Society and the National Institutes of General Medical Sciences (S.R.W.), a Burroughs Wellcome Fund Career Award in the Biomedical Sciences (J.D.Y.), and a Whitehead Scholar Award (J.D.Y.).

29 September 1999; accepted 21 January 2000


# Rapid Extragranular Plasticity in the Absence of Thalamocortical Plasticity in the Developing Primary Visual Cortex


**Joshua T. Trachtenberg, Christopher Trepel, Michael P. Stryker***



**Monocular deprivation during early postnatal development remodels the circuitry of the primary visual cortex so that most neurons respond poorly to stimuli presented to the deprived eye. This rapid physiological change is ultimately accompanied by a matching anatomical loss of input from the deprived eye. This remodeling is thought to be initiated at the thalamocortical synapse. Ocular dominance plasticity after brief (24 hours) monocular deprivation was analyzed by intrinsic signal optical imaging and by targeted extracellular unit recordings. Deprived-eye responsiveness was lost in the extragranular layers, whereas normal binocularity in layer IV was preserved. This finding supports the hypothesis that thalamocortical organization is guided by earlier changes at higher stages.**


The establishment of precise neural circuits is believed to result from activity-dependent rearrangements of neural connections during normal development (*1*). A conventional assumption present in models of visual cortical development and reorganization is that synaptic connections are remodeled serially in the order in which information is processed

(*2*–*4*). An alternative view is that reorganization begins at a higher stage of cortical processing in the extragranular layers, and these higher layers guide changes in both the input layer and subcortical sites (*5*). This latter hypothesis finds support in recent experiments on young kittens and ferrets suggesting that the organization of the supragranular layers precedes the establishment of cortical columns and predicts the subsequent anatomical changes in the geniculocortical afferents (*6*, *7*). The interpretation of these data is not straightforward, however, as these experiments could only infer the late onset of changes in layer IV.

To examine the initial changes in the strength of connections in different layers of the cortex, we studied the loss of cortical response after occluding one eye for 24 ± 1 hours during a critical period in early life in five cats (*8*). Experiments were performed immediately after the termination of the period of monocular deprivation (MD). This short deprivation produced a strong, but not saturated, shift in ocular dominance (OD) that enabled us to measure laminar differences in the onset of plasticity. Two normally sighted kittens (P29 and P33) were used as controls. For each animal, maps of cortical OD were constructed by imaging of intrinsic optical signals (*7*, *9*). These OD maps showed the relative responses of the two eyes, analogous to the OD score of Hubel and Wiesel (*10*), by comparing the best response in either eye to the response with the same stimulus in the other eye.

OD maps constructed in this manner were used to target microelectrode penetrations to regions of the cortex expected to show the greatest plasticity, the binocular saddle points that connect peaks of like OD. These binocular regions are known to be taken over by the nondeprived eye after MD, ultimately leaving only islands of deprived-eye response centered around former OD peaks (*3, 7*). To accurately target the placement of microelectrode penetrations to saddle points, we measured OD peaks and specific contours of OD on the maps. Peaks and saddle points of OD were similarly evident in experimental and control animals. The positional stability of these topographic features ensured that the experimental recordings were made at sites whose properties before deprivation were known from the control animals (*11*). Examples of contoured OD maps and the location of targeted penetration sites relative to the contour lines are shown in Fig. 1, A and B, for two control animals and Fig. 1D for an experimental animal. The locations of all experimental and control penetrations are shown parametrically relative to contour lines of OD, saddle points, and peaks of OD in Fig. 1G. There were no significant differences between the placement of electrode penetrations in experimental and control groups (distance to OD peak: control = 397 ± 16 μm, deprived = 369 ± 36 μm; $P = 0.45$; distance to saddle point: control = 115 ± 33 μm, deprived = 175 ± 39 μm; $P = 0.24$; all values reported as mean ± SEM).

Because the experimental and control recordings came from different animals, we studied one additional control animal to ensure that the control data were not sensitive to modest differences in the position of the electrode penetrations. We bracketed the saddle points with penetrations separated by 2 standard deviations of experimental electrode position closer either to the nondeprived eye's peaks of OD or to those of the deprived eye (Fig. 1, F and G). The measured OD was nearly identical over this region.

In each penetration, the OD of single units was determined (*12*). Two to three electrolytic lesions (3 to 5 μA for 3 to 5 s) were made along each track as the electrode advanced from the pial surface to the white matter. Cells were assigned to one of four cortical layers (II/III, IV, V, and VI) on the basis of reconstructions of the electrode paths in Cresyl violet–stained sections. A total of 187 cells were recorded in deprived kittens: 73 from layer II/III, 48 from layer IV, 35 from layer V, and 31 from layer VI. In control kittens, a total of 155 cells were recorded: 48 from layer II/III, 29 from layer IV, 34 from

W. M. Keck Foundation Center for Integrative Neuroscience and Department of Physiology, University of California, San Francisco, CA 94143–0444, USA.

*To whom correspondence should be addressed. E-mail: stryker@phy.ucsf.edu

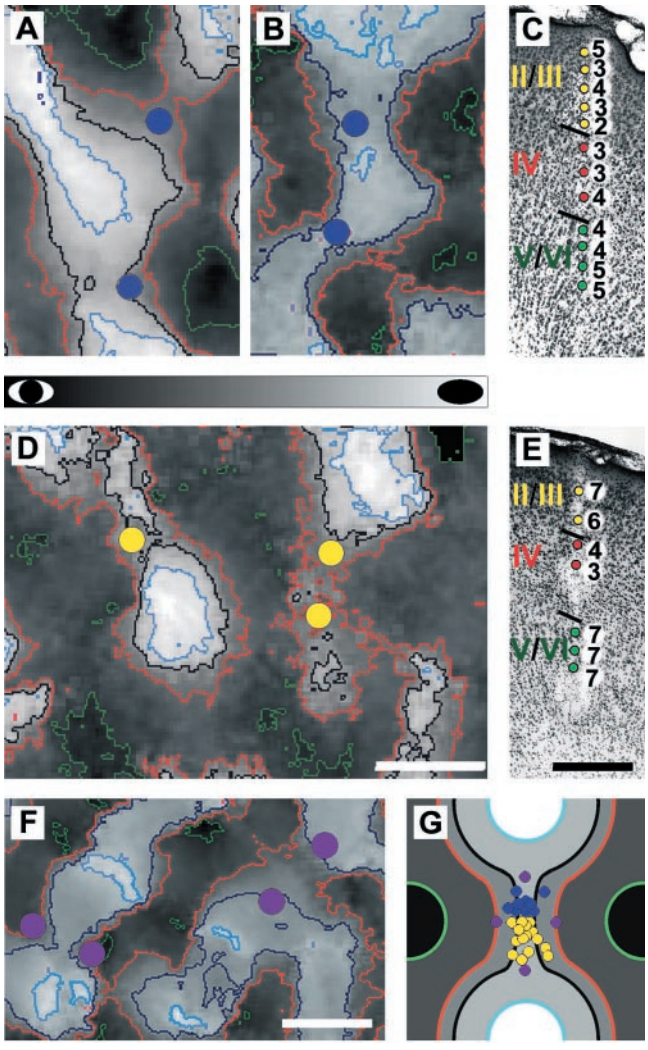


**Fig. 1.** Contoured optical maps of OD used to guide the placement of microelectrodes and electrophysiological responses recorded from such targeted penetrations. (**A** and **B**) Maps from normally sighted, control kittens. (**D**) Map from a kitten that underwent 24 hours of monocular lid suture. Dark regions of the maps were dominated by the nondeprived eye in experimental kittens and by the right eye in control kittens (see gray bar). Orange contour lines define binocular regions formerly dominated by the deprived eye. In control and deprived animals, microelectrode penetrations (blue and yellow circles, respectively) were placed in regions of the maps that had similar optical responses and topographic position. (**C** and **E**) Electrophysiological responses from a targeted penetration in a control and a deprived kitten, respectively. Cells in layers II/III, IV, and V/VI are color coded yellow, red, and green, respectively. Marking lesions allowed assignment of recording sites to cortical layer. In this and all remaining figures, an OD score of 7 or 1 indicates that cells were driven in exclusively by the nondeprived eye or the deprived eye, respectively (in control kittens by the right or left eye, respectively). (**F**) Example of the placement of microelectrode penetrations (purple dots) relative to contour lines of OD in a third control kitten. These penetrations are 2 standard deviations of electrode position closer to the peaks of OD. (**G**) Schematic diagram depicting the parametric placement of microelectrode penetrations relative to contour lines of OD and distance from saddle points and OD peaks in experimental and control kittens. OD, contour lines, and penetrations in experimental and control cortices are colored as in (A), (B), (D), and (F). Scale bars are 500 μm.

layer V, and 44 from layer VI. Examples of individual penetrations in control and monocularly deprived kittens are shown in Fig. 1, C and E, respectively. A clear shift in OD favoring the nondeprived eye is evident in the extragranular layers of deprived animals, but not in the input layer (IV), whereas cells in all layers of control animals were binocular. Such penetrations were typical. Figure 2 shows the data from all deprived and control animals. Relative to control data, neurons recorded in the extragranular layers of deprived kittens were characterized by a significant shift in OD in favor of the nondeprived eye [$\chi^2(4) > 32.0$ for each comparison, $P < 0.001$] (*13*). Within layer IV, however, no significant shift in OD distribution was observed [$\chi^2(4) = 4.04$, $P = 1.0$] (*13*).

To further quantify the shift in OD, we calculated both an ocular dominance index (ODI) and a monocularity index (MI) for each lamina in control and deprived animals (*14*). These indices were first calculated from the OD scores of cells pooled from all animals. Figure 3, A (ODI) and C (MI), demonstrates large effects of deprivation in all layers except layer IV. OD in layers II/III, V, and VI shifted substantially toward the nondeprived eye, and monocularity was enhanced. No change from control values was seen in layer IV of deprived kittens for either index. In the additional control animal, in which seven electrode penetrations were deliberately directed away from the saddle points, the ODI of the 21 neurons recorded from layer IV differed by only 0.01 between the penetrations closer to the peaks of the deprived eye and those closer to the peaks of the nondeprived eye. This similarity further demonstrates that control data were similar over the entire area of cortex from which the experimental data could have come. Because pooled data can be biased by those penetrations from which large numbers of cells were recorded in particular layers, these indices were recalculated for individual penetrations from which cells in all laminae were recorded [Fig. 3, B (ODI) and D (MI); $n = 10$ and 19 penetrations from control and deprived cats]. Significant shifts in the ODI in favor of the nondeprived eye were observed for the extragranular layers ($P < 0.001$, Mann-Whitney U test), whereas no significant shift from control values was observed in the granular layer ($P = 0.43$, Mann-Whitney U test). Similarly, significant shifts toward greater monocularity were seen in the supragranular and infragranular layers without any significant change from binocularity in layer IV. As with the pooled data, the infragranular layers appeared to be more severely shifted in both of these analyses than the supragranular layers.

In agreement with earlier publications (*15*), we found that a larger shift in OD had occurred in the hemisphere contralateral to the deprived eye than in the ipsilateral hemisphere. However, despite the stronger shift in this hemisphere, layer IV experienced no significant shift in ODI or MI relative to control values (ODI: control = 0.41 ± 0.1, deprived = 0.37 ± 0.06; $P = 0.35$; MI: control = 0.38 ± 0.08, deprived = 0.4 ± 0.1; $P = 0.45$; all values reported as mean ± SEM).

The present findings contradict previous models in which plasticity is initiated in the granular layer and simply magnified in the upper layers, unless this magnification is extreme (*4*). The results reported here support the hypothesis that thalamocortical remodeling is guided by higher cortical stages. This hypothesis has the attractive feature that it allows for a common source of plasticity in the developing and more mature cortex, in which MD can produce significant changes in the extragranular layers without significantly altering layer IV (*16*). This view is also consistent with the finding of extragranular plasticity in adult somatic sensory cortex (*17*).

This finding raises two fundamental questions. First, given that the changes in layer IV no longer appear to be instructive or primary, what then is the role of plasticity in layer IV? We suggest that remodeling of layer IV may be required to provide a firm foundation upon which further progressive refinements of higher stages of the cortical circuitry are based. This hypothesis predicts that changes in extragranular responses made after the period in which layer IV shows plasticity would be reversible; studies of human and experimental amblyopia are consistent with this view (*18*). Second, what mechanisms might

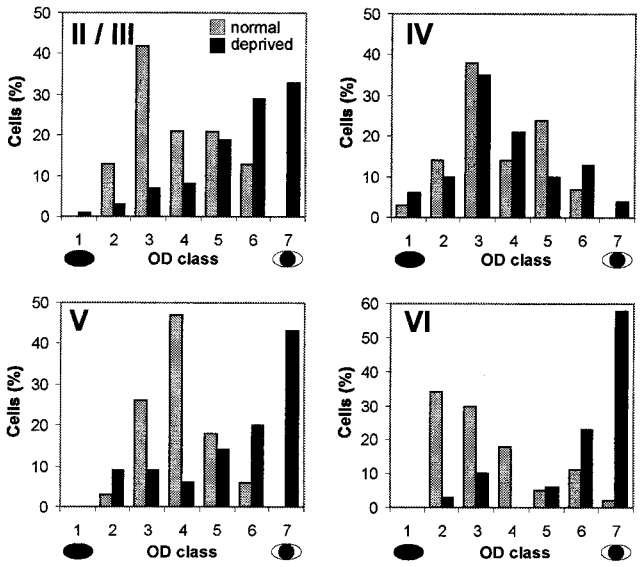


**Fig. 2.** OD histograms constructed from all cells recorded in control (gray bars) and monocularly deprived (black bars) kittens are shown for individual laminae. The laminae are indicated by the number in the top left corner of each histogram. OD scores are as described in Fig. 1. Cells were recorded from both hemispheres and assigned appropriate OD scores. For this analysis, all cells were then rescored as though they had been recorded from the hemisphere contralateral to the deprived eye.

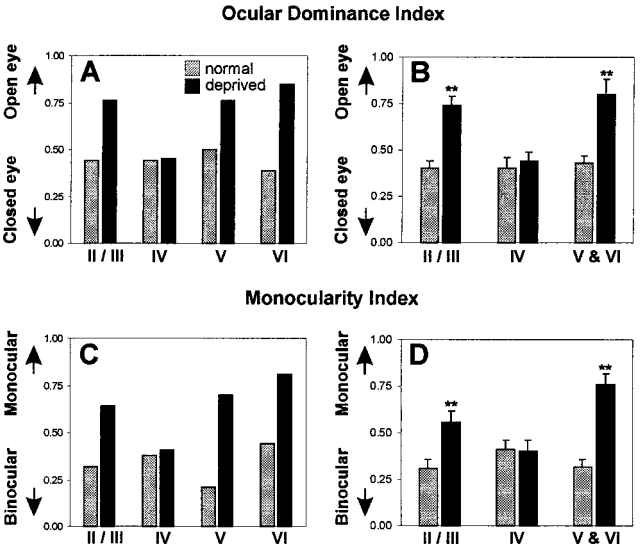


**Fig. 3.** Quantitative analysis of the laminar shifts in OD. Values derived from penetrations in control and monocularly deprived kittens are represented by gray and black bars, respectively. (**A**) Laminar ocular dominance index (ODI) calculated from all cells recorded in each layer. (**B**) Mean laminar ODI (error bars indicate SEM) calculated by averaging the ODI values from cells recorded in each lamina of individual penetrations. (**C**) Laminar monocularity index (MI) calculated from all cells recorded in each layer. (**D**) Mean laminar MIs (error bars indicate SEM) derived by averaging the MIs calculated from cells recorded in each lamina of individual penetrations. Double asterisks in (B) and (D) indicate a statistically significant difference ($P < 0.01$ or greater) from control values. All differences are significant except for layer IV.

initiate remodeling in the extragranular layers? One candidate is a rapid change in the strength of long-range excitatory horizontal connections. Horizontal connections, absent from layer IV (*19*), have been proposed to mediate subthreshold excitation from outside the "classical" receptive field of a cell and, in the absence of strong vertical input, may become capable of driving suprathreshold activity in their targets (*20*). Hebbian learning rules (*21*) might change the strength of horizontal connections between cells dominated by the two eyes. Rapid changes in the efficacy of these connections might produce pronounced shifts in extragranular OD in the absence of a change in input from layer IV.

**References and Notes**


1. L. C. Katz and C. J. Shatz, *Science* **274**, 1133 (1996).
2. M. P. Stryker, *J. Physiol.* **515.P**, 25S (1999) (available at www.physol.org/Proceedings/Abstracts/515P/Cardiff/Files/S201).
3. C. J. Shatz and M. P. Stryker, *J. Physiol.* **281**, 267 (1978).
4. R. D. Freeman and C. Olson, *J. Neurophysiol.* **47**, 139 (1982); K. D. Miller, J. B. Keller, M. P. Stryker, *Science* **245**, 605 (1989).
5. D. V. Buonomano and M. M. Merzenich, *Annu. Rev. Neurosci.* **21**, 149 (1998).
6. E. S. Ruthazer and M. P. Stryker, *J. Neurosci.* **16**, 7253 (1996); M. C. Crair, D. C. Gillespie, M. P. Stryker, *Science* **279**, 566 (1998).
7. M. C. Crair, E. S. Ruthazer, D. C. Gillespie, M. P. Stryker, *Neuron* **19**, 307 (1997).
8. All deprivations and recordings were carried out between postnatal days 27 and 33.
9. Values for individual pixels in the OD maps were computed from each pixel of the unfiltered, blank-normalized images by comparing the response strengths to stimulation of the two eyes at the orientation producing the greatest response. This procedure is similar to that used to determine OD in single-unit recordings, where the responses to optimal stimuli in the two eyes are compared. It is different from the conventional OD ratio maps, which compare the average, rather than the optimal, responses.
10. D. H. Hubel and T. N. Wiesel, *J. Physiol.* **160**, 106 (1962).
11. Comparison of single-unit and optical imaging data in the deprived animals demonstrates that the optical signals reflected a large contribution from activity in layer IV. This is consistent with the reduced thickness of the upper layers at the crown of the gyrus and the scant myelination of the cortex at this age, leading to little light scatter, as well as with the narrow depth of field of the tandem lens optical system focused within layer IV at a depth of 400 μm, leading to a more than sixfold reduction in the contrast of structures the size of OD columns in the upper 100 μm of cortex. D. Malonek *et al.* (*22*) report a 25% contribution from a depth of 800 μm in monkey cortex with similar imaging optics; the layer IV contribution to the optical signal in our experiments would be expected to be at least two times as great.
12. The OD of single units was assessed on the conventional 1-to-7 scale of (*10*). Classification of OD was done blind; that is, one experimenter who was unable to observe the animal because of an interposed screen classified cells as binocular (OD = 4), one category off center in favor of the first or second eye (OD = 3 or 5), two off center (OD = 2 or 6), or an extreme (OD = 1 or 7). Manipulation of the individual eye shutters was performed by the second experimenter, who also recorded the OD rating provided by the first experimenter.
13. $\chi^2$ values were calculated from raw data. As we compressed the standard seven-bin histograms into five bins, the $\chi^2(n - 1)$ statistic had four degrees of freedom. This adjustment was made because we recorded neither cells in extreme OD categories during control experiments nor closed-eye dominant cells from experimental animals.
14. Whereas OD ranking classifies the ratio of contralateral to ipsilateral eye input to a single unit, the ODI measures the degree to which the entire population of units is dominated by the nondeprived eye (or right eye in controls). For cells recorded in the hemisphere ipsilateral to the deprived eye, the ODI is calculated as

$$\mathrm{ODI} = \frac{(N_1 - N_7) + \frac{2}{3}(N_2 - N_6) + \frac{1}{3}(N_3 - N_5) + N_T}{2N_T}$$

whereas for cells recorded in the hemisphere contralateral to the deprived eye, the index equals 1 − ODI. In this equation, $N_T$ is the total number of visually responsive units, and $N_x$ is the number of units with OD rating $x$. An ODI of 0 indicates that the deprived eye dominates the population of measured units, whereas an ODI of 1 indicates that the nondeprived eye dominates the population. This index is designed so that a one-category error in the assessment of OD would cause the same change in the value of the ODI no matter in which OD category it occurs. The MI reflects the degree to which cortical responses are dominated by one eye or the other but not by both. The MI is defined as

$$\mathrm{MI} = \frac{(N_1 + N_7) + \frac{2}{3}(N_2 + N_6) + \frac{1}{3}(N_3 + N_5)}{N_T}$$

An MI of 0 suggests that all individual cells are driven equally by both eyes, whereas an MI of 1 suggests that all cells are driven exclusively by one eye or the other. These indices are similar to those described in (*23*).
15. C. Olson and R. D. Freeman, *J. Neurophysiol.* **38**, 26 (1975); J. A. Movshon and M. R. Dursteler, *J. Neurophysiol.* **40**, 1255 (1977).
16. N. W. Daw, K. Fox, H. Sato, D. Czeptia, *J. Neurophysiol.* **67**, 197 (1992).
17. M. E. Diamond, W. Huang, F. F. Ebner, *Science* **265**, 1885 (1994). This somatic sensory cortical phenomenon differs from that found here in that it lacks a critical period, is not the first stage of an anatomical reorganization, and represents an increase in response strength rather than a loss of response.
18. D. E. Mitchell, *Philos. Trans. R. Soc. London Ser. B Biol. Sci.* **333**, 51 (1991).
19. C. D. Gilbert and T. N. Wiesel, *Nature* **280**, 120 (1979).
20. C. D. Gilbert, *Physiol. Rev.* **78**, 467 (1998).
21. D. O. Hebb, *The Organization of Behavior. A Neuropsychological Theory* (Wiley, New York, 1949); G. Hess, C. D. Aizenman, J. P. Donoghue, *J. Neurophysiol.* **75**, 1765 (1996); D. F. Friedman, G. Hess, J. P. Donoghue, M. S. Rioult-Pedotti, *Nature Neurosci.* **1**, 230 (1998); S. Löwel and W. Singer, *Science* **255**, 209 (1992).
22. D. Malonek, D. Shoham, E. Ratzlaff, A. Grinvald, paper presented at the 20th Annual Meeting of the Society for Neuroscience, St. Louis, MO, 28 October 1990.
23. H. Reiter and M. P. Stryker, *Proc. Natl. Acad. Sci. U.S.A.* **85**, 3623 (1986).


24. Supported by NIH grant R37-EY02874 to M.P.S., a National Research Service Award (EY06824) to J.T.T., and Natural Sciences and Engineering Research Council of Canada and Fight for Sight (research division of Prevent Blindness America) postdoctoral fellowships to C.T.

21 July 1999; accepted 17 January 2000


# Retinal Stem Cells in the Adult Mammalian Eye


**Vincent Tropepe,[1] Brenda L. K. Coles,[1] Bernard J. Chiasson,[1] D. Jonathan Horsford,[2,4] Andrew J. Elia,[5] Roderick R. McInnes,[2,3,4] Derek van der Kooy[1]***



**The mature mammalian retina is thought to lack regenerative capacity. Here, we report the identification of a stem cell in the adult mouse eye, which represents a possible substrate for retinal regeneration. Single pigmented ciliary margin cells clonally proliferate in vitro to form sphere colonies of cells that can differentiate into retinal-specific cell types, including rod photoreceptors, bipolar neurons, and Müller glia. Adult retinal stem cells are localized to the pigmented ciliary margin and not to the central and peripheral retinal pigmented epithelium, indicating that these cells may be homologous to those found in the eye germinal zone of other nonmammalian vertebrates.**


The two functional components of the rodent retina, the inner neural retina (NR) and the outer retinal pigmented epithelium (RPE), are largely developed by the early postnatal period and show no evidence for adult regeneration (*1–3*). These developmental characteristics differ from other vertebrate species in which NR cells are produced throughout life (*4*) and show a remarkable regenerative capacity following injury (*5*). Thus, it has been generally assumed that the adult mammalian eye is devoid of retinal stem cells (self-renewing and multipotential cells) (*6, 7*) and is incapable of substantial neural regeneration. To determine if a stem cell exists in the mouse eye, we examined the ability of single NR cells and single pigmented cells from the entire RPE layer (including pigmented cells from the ciliary margin) (Fig. 1A) to clonally proliferate in vitro using a neural stem cell colony–forming assay (*6, 8*). Dissociated cells from the RPE and the NR were obtained from adult (2 to 3 months old) and embryonic day 14 (E14) mouse eyes and were cultured independently in serum-free media either without exogenous growth factors or in the presence of epidermal growth factor (EGF) or basic fibroblast growth factor (FGF2) (*6, 8*). A small number of individually identified single adult RPE cells (*8*) clonally proliferat-